Journal of Hyperbolic Differential Equations

HIGH RESOLUTION SOLUTIONS FOR THE SUPERSONIC FORMATION OF SHOCKS IN TRANSONIC FLOW

ALLEN M. TESDALL

Mathematics Department, College of Staten Island, City University of New York
Staten Island, New York 10314, United States
allen.tesdall@csi.cuny.edu

Received (Day Mth. Year)
Revised (Day Mth. Year)

Communicated by [editor]

Abstract. We present numerical solutions of two problems for the unsteady transonic small disturbance equations whose solutions contain shocks. The first problem is a two-dimensional Riemann problem with initial data corresponding to a slightly supersonic flow hitting the corner of an expanding duct at $t = 0$. The second problem is a boundary value problem that describes steady transonic flow over an airfoil. In both cases, the solutions contain regions of supersonic and subsonic flow, and an expansion wave interacts with a sonic line to produce a shock. We use high resolution methods, together with local grid refinement, to investigate the nature of the solution in the neighborhood of the point where the shock forms. We find that the shock originates in the supersonic region as originally proposed by Guderley, and very close to, but not at, the sonic line.

Keywords: shock formation; transonic shock; sonic line.

1. Introduction

Shock waves appear generically in solutions of transonic flow problems when rarefaction waves reflect off of sonic lines. When the flow approaching an airfoil has a high subsonic velocity, for instance, a local supersonic "bubble" typically forms on the airfoil, and the expansion wave generated at the airfoil surface reflects off the sonic line as a compression wave which forms a terminating shock. Another example occurs in the Mach reflection of a weak shock off a wedge, known as Guderley Mach reflection (GMR). Numerical solutions (see [12,14,15]) show that a centered expansion wave is generated by the collision of three shocks at the triple point, and is reflected off a sonic line to form a new shock. This shock hits the Mach shock and creates a new triple point, generating a new expansion fan which again reflects off the sonic line, and a whole cascade of shocks formed by characteristics reflecting off a sonic line is thus formed. A further example was introduced in [13]. There, a problem was studied numerically which is analogous to a shock reflection problem in which the incident shock is replaced by an incident rarefaction wave. Physically,

this problem describes a slightly supersonic flow hitting the corner of an expanding duct at $t = 0$. The rarefaction wave generated at the corner reflects off a sonic line, and again a shock wave forms.

The discussion above has made no mention of the point where the shock that is formed by the reflection of characteristics off a sonic line begins. The exact location of the point where the shock begins is difficult to determine numerically, but in each of the cases described above it appears to be very close to, or at, the sonic line. See Fig. 8 and the inset plot in Fig. 12, for example, for illustrations of this claim for the rarefaction wave problem of [13] and for the transonic airfoil problem described above, respectively. Analogous to these figures, Figure 12(b) in [13] depicts velocity contours and the sonic line near the formation point of the first shock in a Guderley Mach reflection. In this case as in the other two, it is impossible to determine from the depicted numerical solution whether or not the shock begins on the sonic line.

Whether a shock forms on the sonic line or in the supersonic region appears to be an open question. Guderley [5] considered the problem of transonic flow over an airfoil, and observed the following concerning the shock at the rear of the local supersonic region: "One is led to suppose that this shock starts at the sonic line and one could ask whether the neighborhood of the point, at which the shock meets the sonic line, could be described by solutions of the type described here." Guderley was unable to find local solutions describing such a sonic shock formation point, however. This led him to propose that the shock forms in the supersonic region due to coalescence of compression waves emanating from the rear portion of the sonic line. The origin of the shock in Guderley's solution is embedded in the supersonic region, as shown schematically in Fig. 1. A physical interpretation of Guderley's proposed supersonic shock formation solution is that the subsonic region plays the role of a permeable obstacle which deflects streamlines towards the airfoil and causes compression waves, exactly as a concave wall does in the classical problem of supersonic flow over a smooth rigid wall [7]. In contrast to Guderley, Moulden [8] concluded that a solution consisting of a shock beginning on the sonic line is possible. Using a general oblique shock analysis, he argued that this scenario can occur provided that the shock is normal to the streamline through the sonic point. In addition, the shock and the sonic line will be tangential at this point. A mathematical proof or disproof of either possibility, however - shock formation on the sonic line or shock formation in the supersonic region - is lacking.

Many numerical solutions of the transonic airfoil problem are available in the literature, beginning with the type dependent relaxation method results of Murman and Cole [10]. A typical example is given in Fig. 4.2 of [7], and depicts a simulation of transonic flow over a NACA 0012 airfoil at a freestream Mach number equal to 0.8 and an angle of incidence of 1.25°, obtained with an invisicid finite volume scheme using quadratic reconstruction on adaptive unstructured meshes. The numerical solution shown in this figure appears similar to our solution of the transonic airfoil problem (at a different set of conditions) shown in Fig. 12: in each case, the origin of the shock appears to lie on or very close to the sonic line. The numerical solution

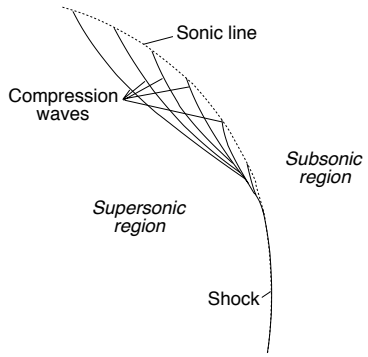

Fig. 1. The behavior of a shock in the vicinity of a sonic line, as proposed by Guderley. The shock originates in the supersonic region due to coalescence of compression waves. A local supersonic region (illustrated here on the left) is generated by an airfoil at high subsonic Mach numbers, and is typically ended by a shock.

displayed in Fig. 4.2 of [7], however, is not sufficiently well resolved to determine whether the shock begins on the sonic line, or near it in the supersonic region. In an early example of a numerical computation of transonic flow, a conservative mixed-type finite difference scheme was developed and used to simulate transonic flow over a parabolic arc airfoil of thickness/length ratio 0.06 at a freestream Mach number equal to 0.85 in [9]. Interestingly, in this pioneering study an attempt was made to determine the nature of the solution near the shock formation point, and the prediction by Guderley of shock formation inside the supersonic region was recognized. The numerical grid resolution, however, was not sufficient to determine whether the shock actually formed in the supersonic region. As stated in [9], "The exact structure at the tip of the shock wave cannot be resolved with the present mesh." To summarize the current situation, numerical solutions of the transonic airfoil problem for high subsonic freestream Mach numbers, at a variety of conditions and using a number of different numerical schemes, show that the shock begins on or very near the sonic line, but we do not know of any which are sufficiently well resolved to be able to distinguish between these two possibilities.

In this paper, we present high resolution numerical solutions of two of our example problems - the rarefaction wave problem of [13], and the problem of steady transonic flow over an airfoil - formulated for the unsteady transonic small disturbance equations (TSDE). We use extreme local grid refinement in the region of the shock formation point (our finest mesh contains approximately 16×10^6 mesh points devoted to the local refinement), together with a high resolution numerical scheme and global grid continuation. Our solutions show that the shock forms strictly inside the supersonic region, as originally proposed by Guderley.

This paper is organized as follows. In Section 2 we summarize the rarefaction wave problem, and describe our approach to solving it numerically. In Section 3 we review the steady transonic airfoil problem and explain the numerical method we

use to solve it. In Section 4 we present our numerical solutions. In Section 5 we discuss our results, and in Section 6 we summarize our findings.

2. The rarefaction wave problem

The rarefaction wave problem was introduced in [13]. It consists of the unsteady transonic small disturbance equations,

$$\begin{aligned} u_t + \left(\frac{1}{2}u^2\right)_x + v_y &= 0, \\ u_y - v_x &= 0, \end{aligned} \tag{2.1}$$

in the half space $y > 0$, together with initial data given by

$$(u, v) = \begin{cases} (0, 0) & \text{if } x > -by, \\ (-1, -b) & \text{if } x < -by, \end{cases} \tag{2.2}$$

and the no-flow boundary condition on $y = 0$,

$$v(x, 0, t) = 0. \tag{2.3}$$

Here, the parameter $b > 0$. The problem (2.1)–(2.3) is self-similar, so the solution depends only on the similarity variables

$$\xi = x/t, \qquad \eta = y/t.$$

Writing (2.1) in terms of ξ and η, we get

$$\begin{aligned} -\xi u_\xi - \eta u_\eta + \left(\frac{1}{2}u^2\right)_\xi + v_\eta &= 0, \\ u_\eta - v_\xi &= 0. \end{aligned} \tag{2.4}$$

Equation (2.4) is hyperbolic when $u < \xi + \eta^2/4$, corresponding to supersonic flow in a self-similar coordinate system, and elliptic when $u > \xi + \eta^2/4$, corresponding to subsonic flow. The equation changes type across the sonic line given by

$$\xi + \frac{\eta^2}{4} = u(\xi, \eta). \tag{2.5}$$

We define a "sonic function" $S = u - (\xi + \eta^2/4)$. When $S < 0$, the flow is supersonic, and when $S > 0$, the flow is subsonic. In the supersonic, hyperbolic region, the inverse slopes of the characteristic curves of (2.4) are given by [6]

$$\frac{d\xi}{d\eta} = -\frac{1}{2}\eta \pm \sqrt{\xi + \frac{1}{4}\eta^2 - u}. \tag{2.6}$$

We refer to the characteristics as plus or minus characteristics, depending on the choice of sign in this equation.

The discontinuity in (2.2) propagates as an expansion wave, giving rise to our description of (2.1)–(2.3) as a rarefaction wave problem for the unsteady TSDE. Where this rarefaction intersects the sonic line (2.5), as shown in [13], a shock is produced, and it is the formation point of this shock that we are focused on in this paper.

2.1. *The numerical method for the rarefaction wave problem*

The basic numerical method we use was developed in [12] in order to solve self-similar problems for the unsteady TSDE, and the numerical boundary conditions needed to solve the rarefaction wave problem were developed in [13]. We describe the numerical method here, and in Section 2.1.1 we outline the numerical boundary conditions used. We also give a full description of the local grid refinement and grid continuation strategies.

The main idea of the numerical method is the introduction of new self-similar variables,

$$\begin{aligned} &r = x/t + \frac{1}{4}(y/t)^2, \qquad \theta = y/t, \qquad \tau = \log t, \\ &\widetilde{u} = u - r, \qquad \widetilde{v} = v - \frac{1}{2}\theta u. \end{aligned} \tag{2.7}$$

Writing (2.1) in terms of the variables in (2.7), we get

$$\begin{aligned} \widetilde{u}_\tau + \left(\frac{1}{2}\widetilde{u}^2\right)_r + \widetilde{v}_\theta + \frac{3}{2}\widetilde{u} + \frac{1}{2}r = 0, \\ \widetilde{u}_\theta - \widetilde{v}_r = 0. \end{aligned} \tag{2.8}$$

Equations (2.8) are identical to the usual unsteady transonic small disturbance equations except for the presence of lower-order terms. Hence, they can be solved by standard methods (in contrast to the situation for the self-similar form (2.4) of the unsteady TSDE.) The advantage of using the self-similar formulation (2.8) instead of the standard, time-dependent formulation (2.1) is that, because the problem (2.1)–(2.3) is self-similar, solutions of (2.8) are stationary. This makes local grid refinement simpler to implement and makes a grid continuation procedure possible.

A fundamental feature of our numerical method is the use of local grid refinement in the area of the shock formation point. We designed a sequence of successively refined, nonuniform, logically rectangular finite difference grids. See Fig. 2 for a diagram of the computational domain (the left and right boundaries of the computational domain are curved because of the use of the parabolic coordinate r in (2.7)). We use grid continuation, in which partially converged coarse grid solutions are interpolated onto more refined grids and converged on those grids. For each grid, inside a given box surrounding the shock formation point, uniform grid spacing is used. Outside of this box the grid is exponentially stretched in both directions.

The basic finite difference scheme is quite standard. Following the classical Cole-Murman approach, we introduce a "velocity" potential $\varphi(r, \theta, \tau)$ such that

$$\widetilde{u} = \varphi_r, \qquad \widetilde{v} = \varphi_\theta,$$

and write (2.8) in the potential form

$$\varphi_{r\tau} + \left(\frac{1}{2}\varphi_r^2\right)_r + \varphi_{\theta\theta} + \frac{3}{2}\varphi_r + \frac{1}{2}r = 0. \tag{2.9}$$

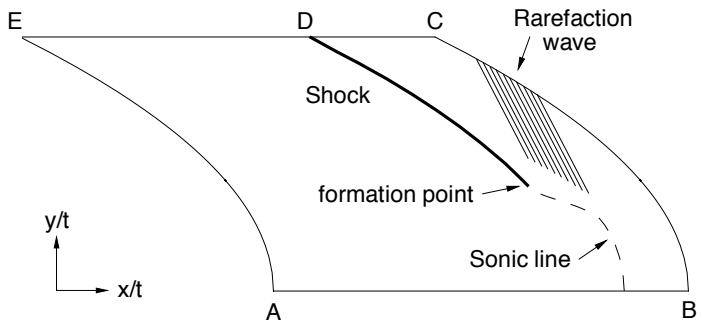

Fig. 2. A schematic diagram of the computational domain. AB is the wall and $BCDEA$ is the numerical boundary. The shock forms in the region where the rarefaction interacts with the sonic line, and exits the computational domain at D. The flow is supersonic in the region to the right of the sonic line, and subsonic to the left of it.

We define a nonuniform grid r_i in the r direction and θ_j in the θ direction, where $r_{i+1} = r_i + \Delta r_i^+$ and $\theta_{j+1} = \theta_j + \Delta\theta_j^+$. We denote an approximate solution of (2.9) by $\varphi_{i,j}^n \approx \varphi(r_i, \theta_j, n\Delta\tau)$, where $\Delta\tau$ is a fixed time step, and we discretize (2.9) in time τ using

$$\frac{\varphi_r^{n+1} - \varphi_r^n}{\Delta\tau} + f(\varphi_r)_r^n + \varphi_{\theta\theta}^{n+1} + \frac{3}{2}\varphi_r^{n+1} + \frac{1}{2}r = 0. \tag{2.10}$$

Here, the flux function f is defined by

$$f(\widetilde{u}) = \frac{1}{2}\widetilde{u}^2. \tag{2.11}$$

To simplify the description, we define discrete "velocities":

$$\widetilde{u}_{i,j} = \frac{\varphi_{i+1,j} - \varphi_{i,j}}{\Delta r_i^+}, \qquad \widetilde{v}_{i,j} = \frac{\varphi_{i,j} - \varphi_{i,j-1}}{\Delta\theta_j^-},$$

where

$$\Delta r_i^+ = r_{i+1} - r_i,$$
$$\Delta\theta_j^\pm = \pm(\theta_{j\pm1} - \theta_j).$$

Then our difference approximation to (2.9) is

$$\frac{\widetilde{u}_{i,j}^{n+1} - \widetilde{u}_{i,j}^n}{\Delta\tau} + \frac{F(\widetilde{u}_{i,j}^n, \widetilde{u}_{i+1,j}^n) - F(\widetilde{u}_{i-1,j}^n, \widetilde{u}_{i,j}^n)}{\Delta r_i^+} + \frac{\widetilde{v}_{i,j+1}^{n+1} - \widetilde{v}_{i,j}^{n+1}}{\frac{\Delta\theta_j^+ + \Delta\theta_j^-}{2}}$$
$$+ \frac{3}{2}\widetilde{u}_{i,j}^{n+1} + \frac{1}{2}r_i = 0. \tag{2.12}$$

Here, F is a numerical flux function consistent with the flux in (2.11). In our computations we used a second order minmod-limited numerical flux based on the Lax-Wendroff and Engquist-Osher numerical fluxes. We solve (2.12) by sweeping

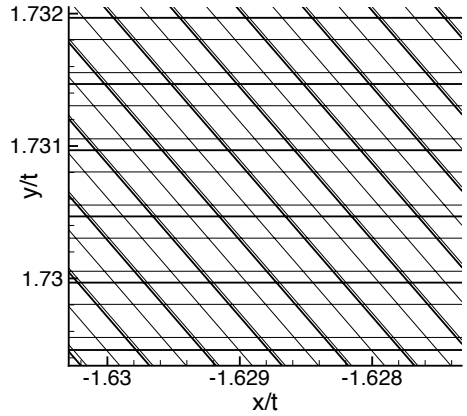

Fig. 3. A coarse grid and a refined grid in the sequence of grids, as they appear in the physical plane $(x/t, y/t)$. The locally refined uniform region of the coarse grid (heavy lines) in this example has $\Delta(x/t) = \Delta(y/t) = 0.0005$, and the fine grid (light lines) has $\Delta(x/t) = \Delta(y/t) = 0.00025$. The region shown is in the uniform grid region of both grids.

from right to left in r. This direction of sweep is consistent with the direction of propagation of the characteristics for (2.4), which is in the $-r$ direction.

We evolve a solution of (2.12) forward in time τ until it converges to a steady state, using line relaxation. For further details of the numerical scheme, see [12].

2.1.1. *The grid and the boundary conditions*

We computed solutions of the problem (2.1)–(2.3) on the finite computational domain $r^L \le r \le r^R, 0 \le \theta \le \theta^T$, shown schematically in Fig. 2. We use a nonuniform grid with a locally refined area of uniformly spaced grid very close to the shock formation point. The grid is stretched exponentially from the edge of the uniform grid region to the outer numerical boundaries and the wall, with a stretching factor of 1%. We note that the grid is orthogonal in the computational plane (r, θ); however, when plotted in physical self-similar coordinates $(x/t, y/t)$, it appears skewed, as shown in Fig. 3.

We use a sequence of such grids, with each grid corresponding to a level of grid refinement. The uniform grid region of each grid is refined by a factor of two in both x/t and y/t with respect to the uniform grid region of the preceding grid. We obtain solutions on coarse grids, interpolate these onto more refined grids, and converge the solutions on the refined grids. We repeat this process until no further change is observed in the solution near the shock formation point, and *grid continue* to a steady state. Figure 3 illustrates the interpolation step of the grid continuation process, and shows a coarse grid (heavy lines) overlayed with a refined grid (light lines) in the uniform grid region of both grids. A solution is obtained on the coarse grid, and the computation on the coarse grid is stopped. This solution is interpolated

onto the refined grid, and the computation is resumed on the refined grid. We found that the amount of computation required to converge a solution on a refined grid was strongly dependent on the type of interpolation used, and we obtained the best results with biquadratic interpolation. Lower order methods such as bilinear interpolation introduced large errors into the interpolated solution, and increased the number of iterations required to converge solutions on refined grids by an order of magnitude or more.

Each grid in the sequence is designed so that the refined uniform grid region surrounds the apparent shock formation point as it appears in the currently available solution (the solution obtained with the previous grid). As the grids are refined and the shock becomes better resolved, the shock formation point can be located more precisely, and the refined grid area can be repositioned and reduced in size.

On the wall boundary AB in Fig. 2 we impose the physical no-flow condition (2.3), which implies that $\varphi_\theta = 0$. In addition, we require numerical boundary conditions on the outer computational boundaries, which we summarize as follows.

The exact solution in the supersonic region far from the origin, as shown in [13], consists of a rarefaction wave with constant states $(u, v) = (0, 0)$ ahead of the rarefaction and $(u, v) = (-1, -b)$ behind it. In terms of the self-similar potential φ, this rarefaction wave solution is given by

$$\varphi(r,\theta) = \begin{cases} -\frac{1}{2}r^2, & \text{if} \quad r > -b\theta + \frac{1}{4}\theta^2 + b^2, \\ \left[\frac{1}{32}\theta^4 - \frac{1}{4}b\theta^3 + (\frac{3}{4}b^2 - \frac{1}{4}r)\theta^2 \right. & \text{if} \quad -b\theta + \frac{1}{4}\theta^2 + b^2 - 1 < r \\ \quad \left. +(br - b^3)\theta - b^2 r + \frac{b^4}{2}\right], & \quad < -b\theta + \frac{1}{4}\theta^2 + b^2, \\ -r - \frac{1}{2}r^2 - b\theta + \frac{1}{4}\theta^2 + b^2 - \frac{1}{2}, & \text{if} \quad r < -b\theta + \frac{1}{4}\theta^2 + b^2 - 1. \end{cases} \tag{2.13}$$

We impose (2.13) as a boundary condition for (2.9) on the supersonic boundary BCD.

The asymptotic behavior of the solution in the subsonic region of the domain at large distances from the origin is given by the solution of the linearized problem in [13]. We use this solution to formulate a numerical boundary condition on the subsonic boundary DEA. In terms of $\varphi_r = \widetilde{u}$, this solution is

$$\varphi_r = -1 - r + \frac{1}{\pi}\left[\tan^{-1}\left(\frac{2\sqrt{-(r+1)}}{\theta - 2b}\right) - \tan^{-1}\left(\frac{2\sqrt{-(r+1)}}{\theta + 2b}\right)\right].$$

Writing this equation as $\varphi_r = f(r, \theta)$, we discretize it as

$$\frac{\varphi_{i+1,j} - \varphi_{i,j}}{\Delta r_{i+1/2}} = f(r_{i+1/2}, \theta_j). \tag{2.14}$$

We impose (2.14) as a Neumann condition on the left subsonic boundary EA, and as a Dirichlet condition on the top subsonic boundary DE.

Further discussion and development of the boundary conditions (2.13) and (2.14) may be found in [13].

3. The steady transonic airfoil problem

We consider the classical problem (see, for example, [1,3,4,10]) of flow over an airfoil with an incoming freestream Mach number which is slightly subsonic. For thin airfoils and small disturbances, the governing equation is the unsteady TSD equation, which can be written

$$\left[\left(1-M_\infty^2\right)\phi_x - \frac{\gamma+1}{2}M_\infty^2\,\phi_x^2\right]_x + \phi_{yy} - 2\phi_{xt} = 0. \tag{3.1}$$

Here, $\phi(x,y)$ is the disturbance velocity potential, where $u=\phi_x$ and $v=\phi_y$ are the disturbance velocity components in the x and y directions, respectively; M_∞ is the freestream Mach number; and γ is the ratio of specific heats. We assume a steady flow, so that (3.1) reduces to the steady TSD equation,

$$\left[\left(1-M_\infty^2\right)\phi_x - \frac{\gamma+1}{2}M_\infty^2\,\phi_x^2\right]_x + \phi_{yy} = 0. \tag{3.2}$$

We consider the case of a symmetric airfoil aligned with the freestream, so that the flow fields above and below the airfoil are symmetric, and there is no lift. The airfoil shape is described by a function $y=F(x), a\le x\le b$.

The boundary value problem for a symmetric non-lifting airfoil in a slightly subsonic freestream flow consists of (3.2), together with boundary conditions that impose the conditions of flow tangency at the airfoil surface, and undisturbed flow at large distances from the airfoil. This boundary value problem is depicted schematically in Fig. 3. We place the airfoil along the x-axis. In the small disturbance approximation, the condition of flow tangency at the airfoil surface is expressed by

$$v = \phi_y = F'(x). \tag{3.3}$$

Following the usual thin airfoil approximation, we apply this boundary condition on a slit at $a\le x\le b$, $y=0$, rather than on the actual body contour, as indicated. By symmetry of the flow field with respect to $y=0$, $\phi_y=0$ on $x<a$, $x>b$, $y=0$.

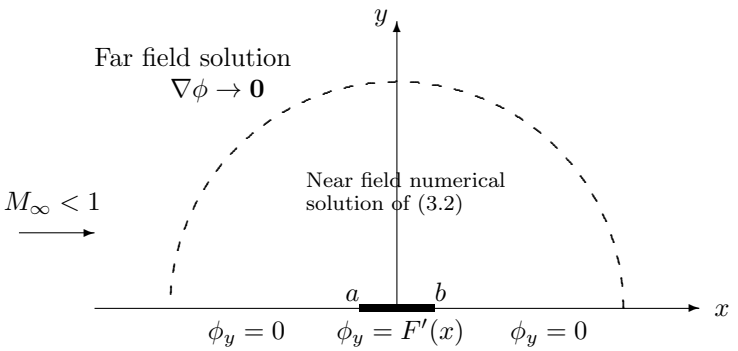

Fig. 4. A schematic diagram of the boundary value problem for (3.2) that describes steady transonic flow over a non-lifting symmetric airfoil. The airfoil is located at $a\le x\le b, y=0$.

Finally, the far field boundary condition

$$\nabla\phi \to \mathbf{0} \quad \text{as } r = \sqrt{x^2+y^2} \to \infty \tag{3.4}$$

expresses the requirement that $u, v \to 0$ at large distances from the airfoil, as indicated in Fig. 3.

For a given airfoil shape function $F(x)$, the problem (3.2)–(3.4) depends on the single parameter M_∞. For M_∞ in the range $M_{cr} < M_\infty < 1$, a supersonic bubble will occur on the airfoil. Here, the critical Mach number M_{cr} is the onset flow Mach number at which the local Mach number somewhere in the flow first reaches 1.

We note that (3.2) is hyperbolic when $\phi_x > (1-M_\infty^2)/[(\gamma+1)M_\infty^2]$, corresponding to supersonic flow, and elliptic when $\phi_x < (1-M_\infty^2)/[(\gamma+1)M_\infty^2]$, corresponding to subsonic flow. The equation changes type across the sonic line given by

$$\phi_x = \frac{1-M_\infty^2}{(\gamma+1)M_\infty^2}. \tag{3.5}$$

3.1. *The numerical method for the transonic airfoil problem*

Our numerical method is similar to the method described in section 2.1, and is based on the time-dependent TSD equation (3.1), since very efficient methods for its solution are available. We define a nonuniform grid x_i in the x direction and y_j in the y direction, where $x_{i+1} = x_i + \Delta x_i^+$ and $y_{j+1} = y_j + \Delta y_j^+$. We discretize (3.1) in time using

$$f(\phi_x)_x^n + \phi_{yy}^{n+1} - 2\,\frac{\phi_x^{n+1}-\phi_x^n}{\Delta t} = 0,$$

where the flux function f is defined by

$$f(u) = \left(1-M_\infty^2\right)u - \frac{\gamma+1}{2}M_\infty^2\,u^2. \tag{3.6}$$

We define discrete velocities

$$u_{i,j} = \frac{\phi_{i,j}-\phi_{i-1,j}}{\Delta x_i^-}, \qquad v_{i,j} = \frac{\phi_{i,j}-\phi_{i,j-1}}{\Delta y_j^-},$$

where

$$\Delta x_i^- = x_i - x_{i-1}, \qquad \Delta y_j^\pm = \pm(y_{j\pm1} - y_j).$$

Our difference approximation to (3.1) is then

$$\frac{F(u_{i,j}^n, u_{i+1,j}^n) - F(u_{i-1,j}^n, u_{i,j}^n)}{\Delta x_i^-} + \frac{v_{i,j+1}^{n+1} - v_{i,j}^{n+1}}{\frac{\Delta y_j^+ + \Delta y_j^-}{2}} - 2\,\frac{u_{i,j}^{n+1}-u_{i,j}^n}{\Delta t} = 0, \tag{3.7}$$

where F is a numerical flux function consistent with (3.6). As in section 2.1, we use a second order minmod-limited numerical flux based on the Lax-Wendroff and Engquist-Osher numerical fluxes. We advance a solution of (3.7) forward in time t until it converges to a steady state, sweeping from left to right in x.

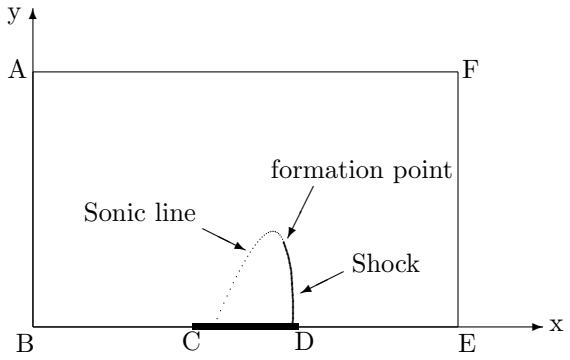

Fig. 5. The computational domain for the transonic airfoil problem. CD is the airfoil. The flow is supersonic inside the "bubble" over the airfoil, and subsonic outside it.

3.1.1. *The grid and the boundary conditions*

We computed solutions of the boundary value problem (3.2)–(3.4) on the finite computational domain depicted in Fig. 5. We use exactly the same strategies of local grid refinement and grid continuation as described in section 2.1.1. For each grid, inside a small region surrounding the shock formation point, uniform grid spacing is used. Outside of this region the grid is exponentially stretched in both directions.

On the airfoil surface CD, we apply the physical flow tangency condition (3.3). In addition, we require numerical boundary conditions on the far field boundary $EFAB$, and on the symmetry boundary $BC \cup DE$. Well-posed and stable far field numerical boundary conditions for transonic flow are well known (see [2], for example). We impose boundary conditions on the far field boundaries which approximately enforce the no-disturbance at infinity boundary condition (3.4), while also ensuring overall conservation of mass. On the upstream boundary AB and the downstream boundary EF we impose

$$\phi_x = 0,$$

and on the sidewall AF we impose

$$\phi_y = 0.$$

We note that each of these boundaries are subsonic. Finally, we impose the symmetry boundary condition $\phi_y = 0$ on the symmetry boundaries BC and DE.

4. Numerical results

We first present our results for the rarefaction wave problem described in Section 2, and follow with a presentation of the results for the transonic airfoil problem described in Section 3.

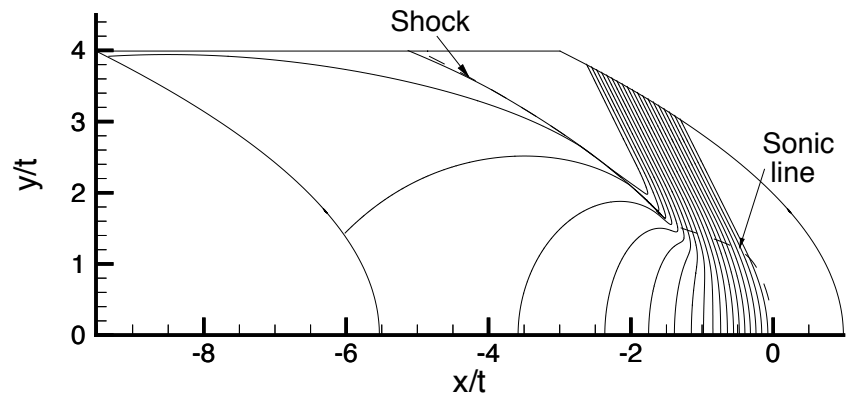

Fig. 6. A contour plot of u-velocity over the full numerical domain. The rarefaction wave enters the computational domain through the right boundary. The dashed line is the sonic line: flow to the right of the sonic line is supersonic, and to the left it is subsonic. The u-contour spacing is 0.05. The full grid contains 5200×5400 grid points.

4.1. *Numerical results I: the rarefaction wave problem*

We computed a numerical solution of (2.1)–(2.3) for b equal to 0.5, using a sequence of ten grids as described in Section 2.1.1. The total number of grid points in our finest grid is approximately 28×10^6, of which 16×10^6 are devoted to the local refinement. We give our finest grid results in the plots which follow. Figure 6 is a contour plot of u-velocity as a function of $(x/t, y/t)$ which gives an overall impression of the solution. The dashed line in the plot is the numerically computed location of the sonic line (2.5). (This sonic line is displayed more clearly in Fig. 8). The shock that is formed by the reflection of the rarefaction wave from the sonic line is clearly visible. To demonstrate that this is a shock and not a continuous compression, in Fig. 7 we plot cross sections of the sonic function S taken horizontally across the apparent discontinuity at $y/t = 3$, $y/t = 2.5$, and $y/t = 2$, from the numerical data. As the shock is crossed from right to left in x/t, in the direction of the flow, S jumps from supersonic (negative) values to subsonic (positive) values, as shown, so the shock is a transonic shock. These cross sections do not show what happens very close to the point where the shock forms, which occurs at a smaller value of y/t than those shown here.

Figure 8 is an enlargement of the solution shown in Fig. 6 in a small region close to the apparent formation point of the shock, where local grid refinement was performed. The dashed line in the plot is the sonic line (2.5). From this figure, the shock appears to begin on or very close to the sonic line. In order to determine where the shock begins, in Fig. 9 we plot cross sections of the sonic function S taken horizontally across the shock at six closely spaced values of y/t which lie in the region shown in Fig. 8. The increasing step size between data points that is

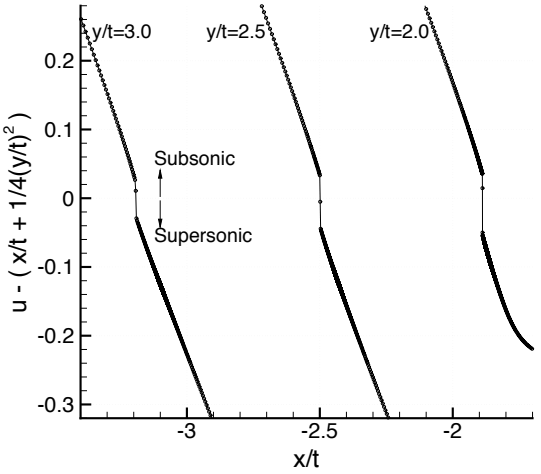

Fig. 7. Cross sections of the sonic function S taken across the shock at three different y/t locations. The flow is supersonic ahead of the shock and subsonic behind it, with flow close to sonic on either side. The high-resolution numerical method captures the shock in one to two points, as shown.

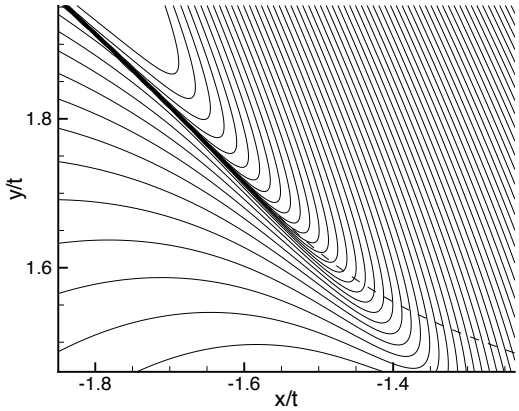

Fig. 8. A contour plot of u close to the shock formation point. The flow is supersonic to the right of the sonic (dashed) line, and subsonic to the left. The u-contour spacing is 0.0075. The region shown contains the refined uniform grid, which has 4000×4000 grid points ($\Delta(x/t) = \Delta(y/t) = 5\times10^{-6}$).

visible near the tails of the curves in this plot is due to the use of a stretched grid. Proceeding in the direction of decreasing y/t, the cross sections at $y/t = 1.77$ and $y/t = 1.76$ (curves **a** and **b**) resemble those shown in Fig. 7 - the shock is transonic at these locations. At $y/t = 1.751$, however (curve **c**), the flow is nearly exactly sonic behind the shock, as shown, and at $y/t = 1.746$ and $y/t = 1.742$ (curves **d** and **e**) the flow is supersonic behind the shock. Curve **f**, corresponding to $y/t = 1.738$,

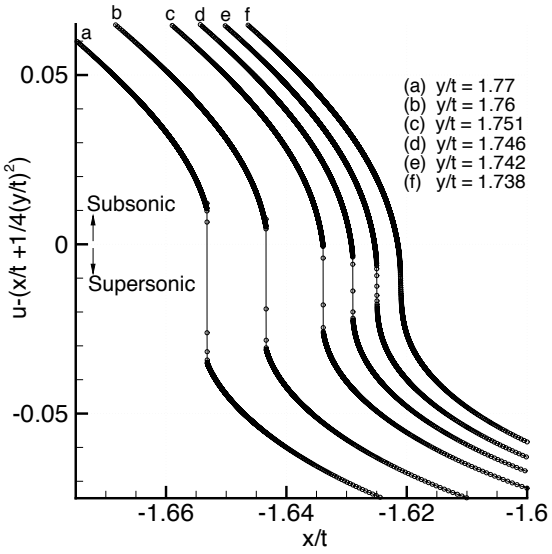

Fig. 9. Cross sections of the sonic function S taken horizontally across the shock near the formation point. The shock has already formed at $y/t = 1.742$ in the supersonic region, but is extremely weak. It remains supersonic for a short distance, becoming exactly sonic at approximately $y/t = 1.751$ and transonic thereafter.

shows that at smaller values of y/t the shock disappears entirely, becoming a steep compression wave. Hence, interpolating the data depicted in curves **e** and **f** shows that the shock forms in the supersonic region at approximately $y/t = 1.740$. It is supersonic from the formation point at $y/t = 1.740$ to approximately $y/t = 1.751$, and transonic thereafter.

Equation (2.4) has two families of characteristics in the supersonic region, and their inverse slopes are given by (2.6). Figure 10 shows the numerically computed characteristic vector fields of the solution in a tiny region in the vicinity of cross section **d** ($y/t = 1.746$), which is approximately midway along the length of the supersonic portion of the shock. The shock, although supersonic here, lies very close to the sonic line, as shown in the plots. The minus characteristics reflect off the sonic line and converge on the shock, while the plus characteristics cross the shock, so the shock is a minus shock. From Fig. 9, we know that the shock becomes sonic at approximately $y/t = 1.751$, and Fig. 11 shows the numerically computed characteristic vector fields near this location. The supersonic shock merges smoothly with the sonic line at a value of y/t close to the predicted value of 1.751, as shown. These characteristic vector field plots are further interpreted in Section 5.

Figures 9, 10 and 11 illustrate that the shock is supersonic for only a short portion of its length, and that it protrudes only a small distance into the supersonic region of flow. Table 1 gives numerical estimates of these lengths when $b = 0.5$, from the numerical data. The approximate locations of the shock formation point

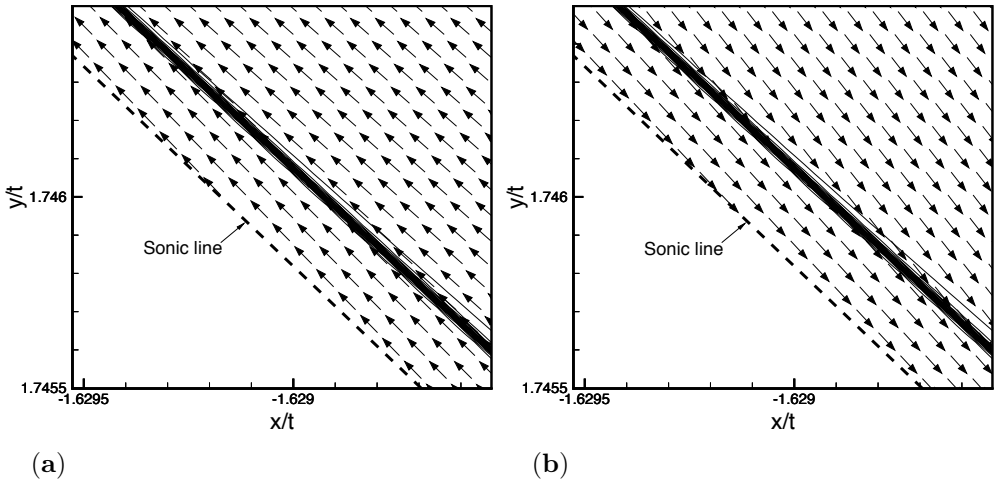

Fig. 10. The minus (a) and plus (b) characteristic vector fields in the region where the shock is supersonic, near where it forms. The shock is the dark band of u-contours. At $y/t \approx 1.740$ (below the region shown in (a) and (b)) the shock forms in the supersonic region, and at $y/t \approx 1.751$ (above the region shown in (a) and (b)) the shock merges with the sonic line (see Fig. 11).

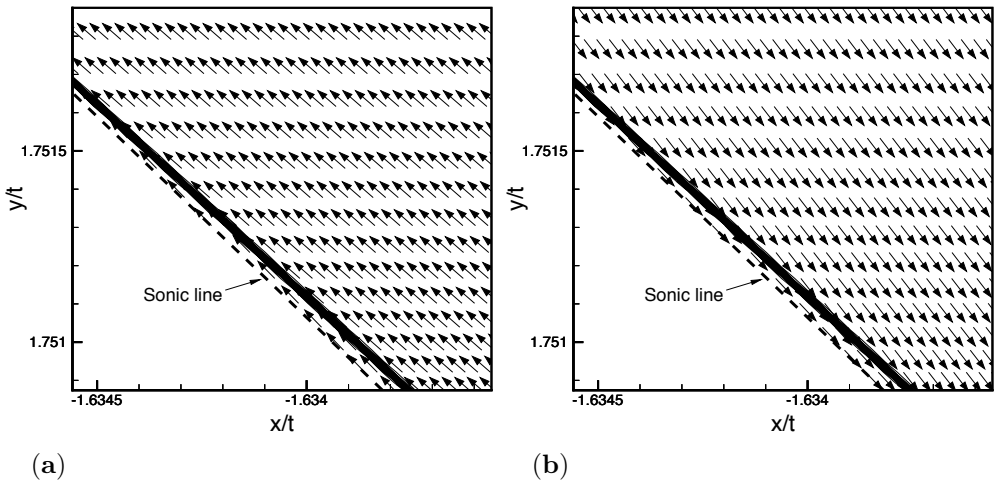

Fig. 11. The minus (a) and plus (b) characteristic vector fields near where the shock merges with the sonic line and becomes transonic.

and the point where the shock merges with the sonic line are given in the table. The supersonic shock length L is a linear estimate of the length of shock between these two points. The distance of penetration $\Delta(x/t)$ into the supersonic region at the formation point is an estimate of the distance from the shock to the sonic line at the value of y/t where the shock forms ($y/t = 1.740$).

Table 1. Numerically computed values of the supersonic shock length L, the distance of penetration into the supersonic region $\Delta(x/t)$, and the locations of the shock formation point and the point where the shock becomes sonic (denoted by the subscripts $_{f.p.}$ and $_{s.p.}$, respectively), for $b = 0.5$.

L	$\Delta(x/t)$	$(x/t)_{f.p.}$	$(y/t)_{f.p.}$	$(x/t)_{s.p.}$	$(y/t)_{s.p.}$
0.016	0.0004	-1.6230	1.740	-1.6344	1.7515

4.2. *Numerical results II: the steady transonic airfoil problem*

We computed a numerical solution of (3.2)–(3.4) for a freestream Mach number M_∞ equal to 0.8 and a parabolic arc airfoil, whose equation is given by $y = 2\delta x(1-x), 0 \leq x \leq 1$, where δ is the airfoil thickness ratio. In our computations we used $\delta = 0.12$. We used a sequence of twelve grids in the grid refinement procedure, with the finest grid containing approximately 30×10^6 grid points, of which 16×10^6 are contained in the locally refined region. We give our finest grid results in the following plots. Figure 12 shows a numerical solution which gives an overall picture of the airfoil flowfield. The main plot in the figure shows u-velocity contours of the global solution as a function of (x, y). There is a supersonic bubble over the airfoil, and the shock terminating this bubble is clearly visible. In order to display the location of the supersonic region and the shock more clearly, the inset plot in the figure shows a closeup of the solution in a small region over the airfoil. The dashed line in the inset plot is the numerically computed location of the sonic line (3.5). The expansion wave generated by the airfoil is clearly visible. The shock, which is formed by the reflection of this expansion wave off the sonic line, appears from the inset figure to begin on or very close to the sonic line.

This shock is further illustrated in Fig. 13, which is a plot of the pressure coefficient C_p on the airfoil surface (in the small disturbance approximation, $C_p = -2u = -2\phi_x$). Following the usual convention, $-C_p$ rather than C_p is plotted on the y-axis, explaining the negative jump in y-value as the shock is crossed in the direction of flow (from left to right). The location of the jump in this plot shows that the shock intersects the airfoil surface at $x \approx 0.725$, which is in agreement with the location indicated in the inset plot of Fig. 12. The shock strength, as measured by the jump $[C_p]$ in C_p, is approximately 0.95 at the airfoil surface, where the shock is a normal shock.

From the inset plot in Fig. 12, the shock appears to form at a value of y close to 0.2. In order to determine where the shock actually forms, in Fig. 14 we plot cross sections of the airfoil sonic function $\widetilde{S} = 1 - M_\infty^2 - (\gamma+1)M_\infty^2\phi_x$ taken horizontally across the shock at several closely spaced values of y on either side of this value. Considering first the cross section at $y = 0.180$ (curve **a**), as the shock is crossed from left to right in x, in the direction of flow, $\widetilde{S}$ jumps from supersonic (negative) values to subsonic (positive) values, so the shock is a transonic shock at this location. Proceeding in the direction of increasing y, the shock is also transonic at $y = 0.190$ (curve **b**), as shown. At $y = 0.200$ (curve **c**), however, the flow is nearly exactly sonic

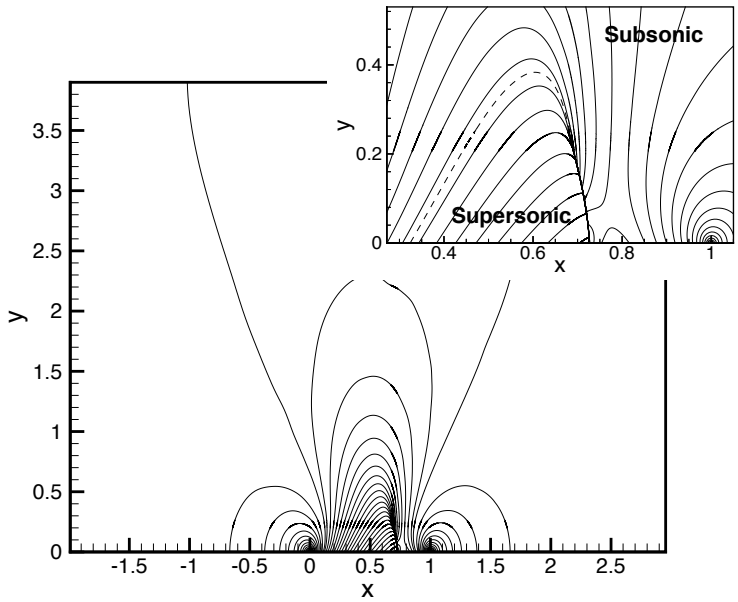

Fig. 12. A contour plot of u-velocity over the full numerical domain, for an $M_\infty = 0.8$ flow at zero angle of attack over a 12% thick ($\delta = 0.12$) parabolic arc airfoil. The airfoil is located at $0 \le x \le 1, y = 0$. The inset plot shows an enlargement of the solution in a region containing the supersonic bubble; the dashed line is the sonic line. The u-contour spacing is 0.02 in the main plot and 0.03 in the inset plot. The full grid contains 5600×5400 grid points.

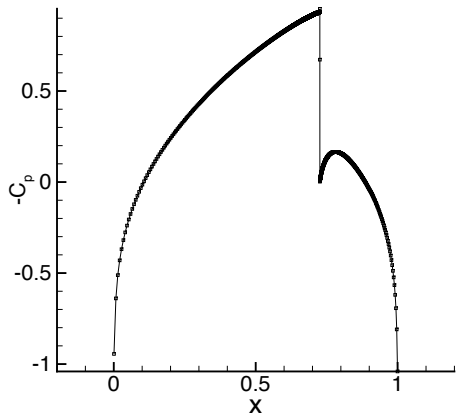

Fig. 13. The negative of the pressure coefficient C_p on the airfoil surface. The jump indicates the location of the shock on the airfoil surface (the airfoil is located at $0 \le x \le 1$). The shock is at approximately 72% of chord, and has strength $[C_p] \approx 0.95$.

behind the shock, and at $y = 0.2075$, $y = 0.215$, and $y = 0.2225$ (curves **d**, **e** and **f**) the jumps are from supersonic to supersonic values, so the shock is supersonic at

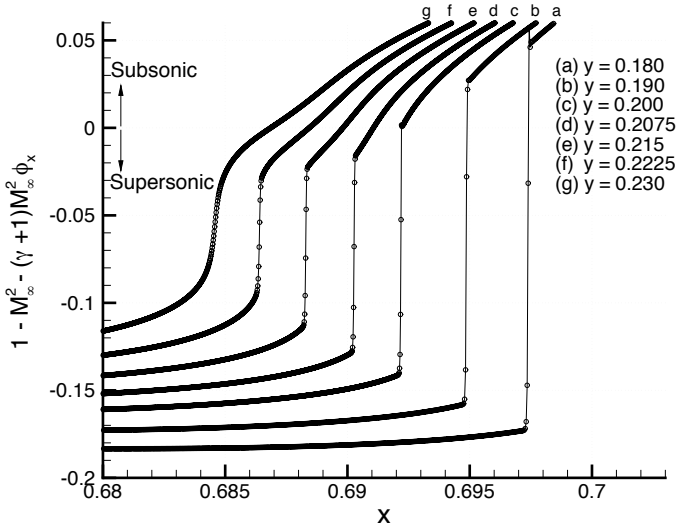

Fig. 14. Cross sections of the airfoil sonic function $\widetilde{S}$ taken horizontally across the shock near the formation point. The shock forms between $y = 0.230$ and $y = 0.2225$ in the supersonic region. It becomes exactly sonic at $y \approx 0.200$, and is transonic for the remainder of its length, hitting the airfoil surface at $y = 0$.

these values of y. Curve **g**, corresponding to $y = 0.230$, shows that at larger values of y the shock disappears entirely, being replaced by a steep compression. Hence, interpolating the data depicted in curves **f** and **g** shows that the shock forms in the supersonic region at a value close to $y = 0.225$. It is supersonic from the formation point at $y \approx 0.225$ to approximately $y = 0.200$, and transonic thereafter until it hits the airfoil surface at $y = 0$ as a normal shock.

In order to provide a more physical depiction of the shock formation situation just described, in Fig. 15 we plot u-contours in a small region close to the formation point of the shock, where local grid refinement was performed. (The region shown in this figure is contained in the larger region depicted in the inset plot of Fig. 12). The dashed line in the plot is the sonic line (3.5). The steepening of a compression wave into a shock at the formation point A ($x \approx 0.686$, $y \approx 0.225$) is clearly visible. The shock is supersonic from point A to point B ($x \approx 0.692$, $y \approx 0.200$), where it merges smoothly with the sonic line and becomes transonic. The total length of the supersonic portion of the shock is approximately 0.026, and the maximum distance that it extends into the supersonic region (as measured by the distance in x from the formation point to the sonic line) is approximately 0.002. These data are summarized in Table 2.

We note the remarkable similarity of the solution in Fig. 15 to Guderley's proposed supersonic shock formation solution in Fig. 1.

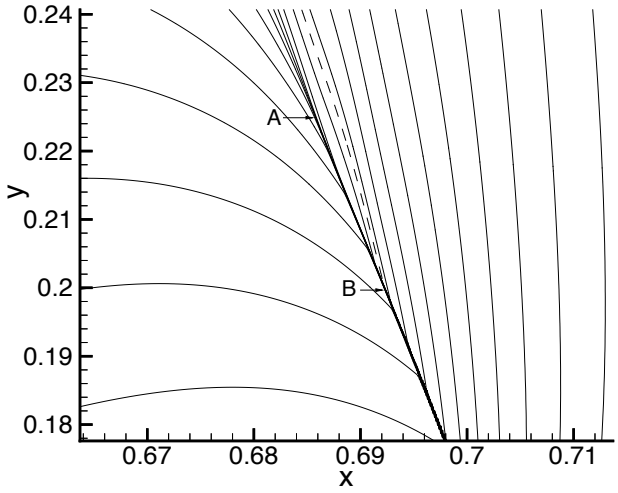

Fig. 15. A closeup of the solution near the shock formation point (point A), showing formation inside the supersonic region. The flow is supersonic to the left of the sonic (dashed) line, and subsonic to the right. The u-contour spacing is 0.01. The region shown contains the locally refined uniform grid, which has 4000×4000 grid points ($\Delta x = \Delta y = 1 \times 10^{-5}$).

Table 2. Numerically computed values of the supersonic shock length L, the distance of penetration into the supersonic region Δx, and the locations of the shock formation point and the point where the shock becomes sonic, for $M_\infty = 0.8$, 12% thick parabolic arc airfoil.

L	Δx	$x_{f.p.}$	$y_{f.p.}$	$x_{s.p.}$	$y_{s.p.}$
0.026	0.002	0.686	0.225	0.692	0.200

5. Discussion

Two features stand out in these numerical solutions. The first is that the shock begins in the supersonic region, and the second is that the length of the supersonic portion of the shock, and the distance that it extends into the supersonic region of flow, are small compared with some characteristic length. For example, in our solution of the transonic airfoil problem at $M_\infty = 0.8$, the length of the supersonic portion of the shock is approximately 10% of the total length of the shock, and the distance from the point where the shock begins in the supersonic region to the sonic line is approximately 0.9% of the total length of the shock. The smallness of these distances is much more striking in our solution of the rarefaction wave problem for $b = 0.5$: there, the length of the supersonic portion of the shock is approximately 0.9% of the height at which the shock begins, and the distance from the shock formation point to the sonic line is approximately 0.02% of the height at which the shock begins. In the case of the steady transonic airfoil problem, these attributes of the shock formation zone - the closeness of the supersonic shock to the

sonic line (see Fig. 15), and the short length of the supersonic shock - explain why the supersonic nature of the shock formation point had not been observed before, despite intensive numerical study.

Since we have obtained a highly refined solution of the airfoil problem only for one particular value of M_∞ and one particular airfoil, we do not know how the length of the supersonic shock and its distance from the sonic line vary as, say, the equation of the airfoil is held fixed while M_∞ is varied over the range of values $M_{cr} < M_\infty < 1$ which result in a supersonic bubble over the airfoil. Similarly, we have obtained a solution of the rarefaction wave problem only for a single value of the parameter b, and do not know how these lengths vary as b varies over the range $b > 0$. Presumably, varying M_∞ in the airfoil problem (while holding the airfoil fixed) or varying b in the rarefaction wave problem would result in longer or shorter supersonic shocks than those observed in our numerical solutions. We do not know, however, whether some set of parameter values in either of these problems results in a supersonic shock length of zero, that is, whether the shock forms exactly on the sonic line as proposed by Moulden [8], instead of in the supersonic region, for some set of parameter values.

We found that more refined grids were required to adequately resolve the solution near the shock formation point for the rarefaction wave problem than for the transonic airfoil problem. This is because the shock in our solution of the rarefaction wave problem begins much closer to the sonic line than does the shock in our solution of the transonic airfoil problem, at the parameter values that we chose for the problems. From Tables 1 and 2, the distance from the shock formation point to the sonic line is 0.0004 (in x/t) in our solution of the rarefaction wave problem and 0.002 (in x) in our solution of the transonic airfoil problem. Because of this, as we obtained solutions of the transonic airfoil problem on successively more refined meshes the apparent shock formation point separated from the sonic line, and became clearly supersonic, at coarser grid resolutions than in the rarefaction wave problem. Our most refined grid for the rarefaction wave problem contains approximately 80 mesh points between the shock formation point and the sonic line ($\Delta(x/t) = \Delta(y/t) = 5 \times 10^{-6}$), while our most refined grid for the transonic airfoil problem contains approximately 200 mesh points between the shock formation point and the sonic line, even with a coarser mesh size ($\Delta x = \Delta y = 1 \times 10^{-5}$). By comparison, in numerical solutions for Guderley Mach reflection [12,14,15], even with the use of highly refined meshes comparable to those used here, the distance between the shock and the sonic line is of the order of the mesh spacing. It does not appear to be feasible, at present, to adequately resolve the formation point of even the first shock in the sequence of reflected shocks in a Guderley Mach reflection.

We note that typical transonic airfoil computations that are of interest to aerodynamicists are for lifting, rather that non-lifting, situations: lift is generated either by non-zero angle of incidence or by non-symmetric airfoils, or by both simultaneously. The reason we solved the non-lifting symmetric airfoil problem described in

Sec. 3 is that this enabled us to use half as many numerical grid points as would be required to solve the lifting problem (where the flow field is not symmetric about $y = 0$) for the same numerical resolution. Because of this resolution issue, the lifting problem would be more computationally intensive, and an additional parameter, angle of incidence, would be introduced. We expect solutions of the lifting problem to be qualitatively similar to the non-lifting solution obtained here, however: we would expect to again find that the shocks above and below the airfoil form in the supersonic region. However, as noted above, we do not know whether some set of parameter values results in a supersonic shock length of zero.

Returning to Fig. 10, two properties of the characteristic vector fields of the solution near the shock formation point are apparent. The first is that the two families of characteristics appear to point in nearly opposite directions near the sonic line, and the second is that both families appear to be approximately tangent to the sonic line. These features may be explained by the following considerations. From equation (2.6), both families of characteristics have the same slope on the sonic line,

$$\frac{d\xi}{d\eta} = -\frac{1}{2}\eta,$$

so the two direction fields point in exactly opposite directions on the sonic line. Hence we expect the two direction fields to point in nearly opposite directions in the neighborhood of the sonic line, as they appear from the figure to do. Differentiating the equation of the sonic line (2.5) with respect to ξ gives the sonic line slope [6],

$$\frac{d\xi}{d\eta} = \frac{-\frac{1}{2}\eta + u_\eta}{1 - u_\xi}.$$

The two characteristic families are almost parallel to the sonic line because u is changing very slowly along the sonic line (note that the u-contours in Fig. 10 are nearly parallel to the sonic line), so that the derivatives on the right side of this equation are small.

6. Conclusion

We have presented numerical evidence of a structure of shock wave formation originally proposed by Guderley. In this structure, a shock wave originates in the supersonic region of flow due to coalescence of compression waves which are reflected from a sonic line. We find that the shock forms very close to the sonic line, and we require the use of extreme local grid refinement and high resolution methods in order to distinguish between the two possibilities of shock formation in the supersonic region, and shock formation exactly on the sonic line.

Acknowledgments

We wish to thank Barbara L. Keyfitz for the idea for the paper, and for valuable discussions and advice.

The author's research was supported by the National Science Foundation, Grant DMS 03-06307, NSERC grant 312587-05, Department of Energy grant DE-SC0001378, PSC-CUNY Research grant 60145-39 40, and the Fields Institute.

References

[1] W. F. Ballhaus and J. L. Steger, Implicit approximate-factorization shemes for the low-frequency transonic equation, *NASA TM-X-73082* (Nov. 1975).
[2] B. Engquist and A. Majda, Numerical radiation boundary conditions for unsteady transonic flow, *J. Comp. Phys.* **40** (1981), 91–103.
[3] B. Engquist and S. Osher, Stable and entropy satisfying approximations for transonic flow calculations, *Math. Comp.* **34** (1980), 45–75.
[4] P. M. Goorjian and R. van Buskirk, Implicit calculations of transonic flows using monotone methods, *AIAA-1981-331*, AIAA 19th Aerospace Sciences Meeting, Jan. 12-15, 1981.
[5] K. G. Guderley, *The Theory of Transonic Flow*, (Pergamon Press, 1962).
[6] J. K. Hunter and M. Brio, Weak shock reflection, *J. Fluid Mech.* **410** (2000), 235–261.
[7] A. G. Kuz'min, *Boundary Value Problems for Transonic Flow*, (Wiley, 2002).
[8] T. H. Moulden, *Fundamentals of Transonic Flow*, (Wiley, 1984).
[9] E. M. Murman, Analysis of embedded shock waves calculated by relaxation methods, *AIAA J.* **12** (1974), 626–633.
[10] E. M. Murman and J. D. Cole, Calculation of plane steady transonic flows, *AIAA J.* **9** (1971), 114–121.
[11] J. von Neumann, *Collected Works*, Vol. 6 (Pergamon Press, 1963).
[12] A. M. Tesdall and J. K. Hunter, Self-similar solutions for weak shock reflection, *SIAM J. Appl. Math.* **63** (2002), 42–61.
[13] A. M. Tesdall and B. L. Keyfitz, A continuous, two-way free boundary in the unsteady transonic small disturbance equations, J. Hyperbolic Differ. Equ. **7** (2010), 317–338.
[14] A. M. Tesdall, R. Sanders, and B. L. Keyfitz, The triple point paradox for the nonlinear wave system, *SIAM J. Appl. Math.* **67** (2006), 321–336.
[15] A. M. Tesdall, R. Sanders, and B. L. Keyfitz, Self-similar solutions for the triple point paradox in gasdynamics, *SIAM J. Appl. Math.* **68** (2008), 1360–1377.